SUFFICIENCY AND NECESSITY OF TUMOR-DERIVED IL6 ON SKELETAL MUSCLE IN PDAC-ASSOCIATED MUSCLE ATROPHY

by

MAYURIKA BHASKAR

A THESIS

Presented to the Department of Chemistry and Biochemistry
and the Robert D. Clark Honors College
in partial fulfillment of the requirements for the degree of
Bachelor of Science

Spring 2024

An Abstract of the Thesis of

Mayurika Bhaskar for the degree of Bachelor of Science
in the Department of Chemistry and Biochemistry to be taken May 2024

Title: Sufficiency and necessity of tumor-derived IL6 on skeletal muscle in PDAC-associated muscle atrophy

Approved: *Carrie McCurdy, Ph.D.*
Primary Thesis Advisor

Approved: *Jesse Feddersen, Ph.D.*
Clark Honors College Faculty Representative

Approved: *Aaron Grossberg, M.D, Ph.D.*
Secondary Thesis Advisor

The most common form of pancreatic cancer, pancreatic ductal adenocarcinoma (PDAC), is one of the most fatal cancers worldwide with an 11.5% 5-year survival rate. Cancer cachexia, defined as a loss in skeletal muscle and fat mass that cannot be regained with nutritional supplementation, is a common morbidity that impacts over 80% of patients with PDAC. Cachexia makes it challenging for patients to receive life-extending treatments and decreases their quality of life. Prior research has shown interleukin 6 (IL6), a pro-inflammatory cytokine, is associated with cancer cachexia development. IL6 acts within its target cells by activating the IL6/JAK2/STAT3 pathway, a signaling pathway that transmits signals from the extracellular environment to the nucleus, leading to changes in gene transcription. In cancer cachexia models, phosphorylation of STAT3 activates skeletal muscle and is a common feature of skeletal muscle wasting. However, we are still unaware of the specific mechanisms by which IL6 causes muscle wasting. I hypothesized that IL6 is sufficient and necessary to induce muscle wasting by acting directly on skeletal muscle. For my honors thesis, I chose to study the potential mechanisms and pathways of IL6 in in vitro C2C12 myotube models and IL6 knock-out (IL6 – KO) and WT mouse models. In the mouse models, PDAC tumors derived from tumors that grow

spontaneously in the transgenic KPC mouse that either did (KPC – IL6 OE) or did not over-express IL6 (KPC – parental) were implanted orthotopically, and myofiber atrophy was documented by measuring the diameter of myofibers and skeletal muscle mass from the harvested gastrocnemius muscle. In vitro, C2C12 myotubes were treated with conditioned media from these cancer cell lines, recombinant IL6 (rIL6), or hyper-IL6 (hIL6, the bound IL6 and IL6-R complex), and myotube atrophy was similarly measured via minimum feret diameter. Activation of the IL6/JAK2/STAT3 pathway by IL6 was measured by quantifying phosphorylated STAT3 in western blot procedures and Socs3 (an indicator of IL6 signaling) product in qPCR using different conformations of IL6. We report that (1) IL6 is necessary and sufficient to drive skeletal muscle mass loss in our mouse models, (2) rIL6 does not induce wasting or activate STAT3 signaling in vitro, and (3) neither rIL6 nor hIL6 is sufficient to drive muscle wasting in vitro, despite activating IL6/JAK2/STAT3 signaling. These results indicate that while IL6 is both sufficient and necessary to induce muscle atrophy in vivo, it does not act directly on the skeletal muscle. Therefore, we conclude that IL6 causes muscle wasting through an indirect signaling mechanism involving other effector cells.

Acknowledgments

I would first like to thank Dr. Grossberg for allowing me to be a part of his lab for the OHSU CDCB internship during the summer of 2022 and the subsequent summer, and for the extensive mentorship and guidance he has given me in successfully writing and defending my thesis. His patience and insight have allowed me to develop my critical thinking and analysis in scientific research and further fostered my love for it. I would also like to thank Paige Arneson-Wissink, Jessica Dickie, and Heike Mendez as members of the Grossberg lab for teaching me the basics of all the experimental procedures and statistical analysis I conducted, their support was instrumental in ensuring I had high-quality, reliable data. I would also like to thank Dr. McCurdy and Dr. Feddersen for serving as members of my committee, they were incredibly helpful in making sure I was not missing any necessary information in my thesis. Additionally, I'd like to thank Dr. Ambati and the Ambati lab's members for taking me in and giving me my first ever glimpse at undergraduate scientific research. They helped establish the foundation for my future pursuits with Dr. Grossberg at OHSU. Also, a special thank you to the OHSU CDCB (Cell, Developmental & Cancer Biology) Summer Internship in 2022 for allowing me to be acquainted with the Grossberg lab and form the integral connections I needed to complete this thesis.

Finally, I would like to thank my amma and appa, Dr. Kirthika Balakrishnan and Bhaskar Uthanumalliah, and my younger sister, Mehneka Bhaskar, for their constant support during my thesis and my 4 years here at the University of Oregon. I would not be the student, woman, and person I am today without any of them.

Table of Contents

List of Figures

List of Diagrams

INTRODUCTION

Pancreatic Cancer

Pancreatic cancer is a form of cancer that originates in the pancreas when pancreas cells mutate and multiply out of control to form a tumor. It makes up about 3% of cancer cases in the United States and globally is the 12th and 11th most common form of cancer worldwide in men and women, respectively. In 2020 alone, there were 495,000 new cases of the disease worldwide (WCRF, 2022), and experts suggest that by 2030, pancreatic cancer will be the second leading cause of cancer death in the United States (Rahib et. al, 2014).

The two most common types of pancreatic cancers are defined by the cell types that form the tumor – exocrine and neuroendocrine. Exocrine and neuroendocrine tumors are composed of malignant exocrine cells (produce digestive enzymes) and neuroendocrine cells (produce blood-sugar stabilizing hormones, i.e. insulin), respectively. In the most diagnosed cases, exocrine tumors account for 90% of pancreatic tumors while neuroendocrine account for the other 10%. Pancreatic ductal adenocarcinoma, or PDAC, is a type of exocrine-tumor pancreatic cancer that develops from cells lining the pancreatic ducts and acini. The most common form of pancreatic cancer, it is also the most lethal, with an average 5-year survival rate of 12% (Siegel et al., 2024). In comparison to other forms of cancer, it ranks fourth in the most frequent causes of cancer-related deaths worldwide (Orth et. al, 2019) largely due to low treatment success rate and late-stage diagnosis (Weledji et. al, 2016).

What makes PDAC so deadly is its intense yet hidden aggressiveness that moves quickly but quietly, making it notoriously difficult to diagnose. Researchers note that there are hardly any early symptoms specific to the disease, largely because the pancreas sits rather deep in the abdomen and is hidden behind other organs, making it difficult to feel for any tumors in routine physical exams or even medical imaging procedures (Grossberg et. al, 2020). It also invades surrounding tissues and organs at a very fast rate) as 50% of PDAC patients are at a metastatic stage when diagnosed while 35% have locally advanced, and therefore unresectable, disease (Weledji et. al, 2016). This is because, in tandem with it being so difficult to observe, it also has a very strong propensity and potential to metastasize compared to most other forms of cancer (Pereira et. al, 2020)

Additionally, the symptoms of the disease itself are commonly overlooked as they are generally nonspecific. The most common ones are symptoms are fatigue, loss of appetite, and weight loss. Due to the lack of specificity of most of these symptoms, these diseases may persist for an extended period before patients are considered for pancreatic cancer, only being treated as just muscular or stomach issues without the pancreas being considered at all. Even when the disease has progressed further, multiple symptoms could be attributed to old age such as fatigue, jaundice, and weight loss (Porta et. al, 2005). In total, this disease is challenging to diagnose early. There are risk factors, such as a social history of smoking, obesity, and diabetes, that are so generalized they often are not enough to warrant further testing for PDAC Grossberg et al., 2020). Additionally, if there exists a family and/or medical history of pancreatic cancer and pancreatitis, early screening for cancers can be considered (Capasso et al., 2018). However, the United States Preventative Services Task Force (USPSTF) recommends against pancreatic cancer screening for the

general population as it is deemed as largely unnecessary (USPSTF, 2019). Overall, however, most pancreatic cancer cases are diagnosed usually later in one's life, either incidentally or when persistent or severe symptoms prompt workup.

Therefore, PDAC is a silent killer as it can invade other tissues, which can cause a multitude of other issues that unfortunately won't manifest right away into distinct, noticeable symptoms so that it can be diagnosed. However, there is a very specific symptom associated with PDAC which while difficult to diagnose, provides a specific avenue to treat the disease: cancer cachexia.

Cancer Cachexia

Cancer cachexia is a complex, multifactorial metabolic disorder that leads to a a significant loss in skeletal muscle and adipose mass that cannot be regained with any nutritional supplementation (Arneson-Wissink, et al., 2022). It is largely driven by decreased food intake and changes in hormones and metabolism regulation, which induce excess catabolism and increased energy usage. This disorder is a major characteristic of multiple cancers in the advanced and/or metastatic stage and accounts for nearly 20% of all cancer deaths (Poulia et al., 2020). This is concerning as it affects 70-80% of PDAC patients (Poulia et al., 2020). Cachexia drastically decreases the quality of life via symptoms such as intense weakness, fatigue, and nausea. These symptoms can exacerbate the effects of different treatments and/or make patients ineligible due to their weakness (Fearon, 2008).

Cancer cachexia is divided into three different stages, depending on the severity of its symptoms. Originally, cachexia could be defined by multiple different factors such as the involuntary weight loss of greater than 5% of a patient's historical weight or a skeletal

mass consistent with sarcopenia (age-related, progressive loss of muscle mass and strength) but leads to weight loss greater than 2% (Fearon et. al, 2011). As research progressed, a more specific categorization of cachexia was developed to denote specific distinctions which led to the classification of 3 cancer cachexia types: pre-cachexia, cachexia, and refractory cachexia. Pre-cachexia is when a patient experiences weight loss of less than 5% but has not yet developed serious symptoms. Cachexia is when the disorder continues to progress and weight loss exceeds the parameters but can still be treated. Finally, refractory cachexia is the latest stage of cachexia where it's no longer responsive to treatments, and any potential treatment benefits are outweighed by the burden/risk (Vaughn et. al, 2013). Regardless, at each stage of cachexia, these truths remain the same: nutritional supplementation alone is insufficient to reverse a cachectic state, and there are no proven pharmacological interventions that can either prevent or reverse said cachectic state (Grossberg et. al, 2020).

The significant negative impact on the quality of life that cancer cachexia has on patients makes it uniquely complex to manage. The detrimental influence it has on quality of life is multidimensional and confers debilitating symptoms that make life more difficult and exhausting to live in comparison to cancer patients without any cachectic symptoms. These symptoms are known to occur in clusters, with the most common being fatigue, overall weakness, a lack of energy, and weight loss (Tsai et. al, 2010). Fatigue is the most common and has the greatest effect on normal activities and quality of life, making a cancer patient's situation significantly more difficult (Ahlberg et. al, 2003). This can manifest into psychosocial issues as it's associated with increased depression, self-consciousness, anxiety, and decreased social engagement (Hopkinson et al., 2006). Therefore, with all

these symptoms combined, cancer cachexia not only develops physical symptoms but also psychological and social ones as well, making it a multimodal disease that can be treated from a variety of treatment types.

It is important to understand cachexia's potential causes from a molecular standpoint when attempting to treat it in a biological, medical content. Cancer cachexia is a complex disorder that involves multiple cytokines, hormones, neuropeptides, and tumor-related factors (Poulia. Et al, 2020). Hallmark symptoms of cancer cachexia, alongside the significant skeletal muscle and adipose tissue loss, include anemia, hypogonadism, insulin resistance, and chronic inflammation (Fearon et. al 2020, White et. al 2013). When specifically looking at chronic inflammation, there have been multiple inflammatory cytokines associated with cachexia such as TNF–α, interleukin-1 (IL-1), and interferon-γ (IFN-γ) as they present in elevated levels in cachectic states (Webster et. al, 2020). But as research progressed, IL6 became a potential target of interest as its levels correlate with the survival time in patients and has been the most associated with cachexia by far (Suh et. al, 2013; Rupert et. al, 2021). Therefore, more work/research has been geared toward figuring out the reason behind these possible connections.

Interleukin-6 & IL6/JAK2/STAT3 Pathway

Interleukin-6, or IL6, is a multifunctional cytokine central in host defense due to its anti/pro-inflammatory-associated immune activities and other metabolic, developmental, and hematopoietic activities (Simpson et. al, 1997). It is also a strong activator of the IL6/JAK2/STAT3 pathway, a signaling pathway that has been shown to play a critical role in cell proliferation and differentiation, and in turn, cancer development and progression (Huang et. al, 2022). The pro-inflammatory and metabolic properties of IL6 and its

involvement in this pathway hold the most significance about its potential interactions and development of cancer cachexia in PDAC.

To activate the IL6/JAK2?STAT3 pathway, IL6 first binds to membrane IL6 receptors (mbIL6-Rs) which then activates non-receptor tyrosine kinases (proteins that add a phosphate group to other molecules) such as Janus kinase 2 (JAK2) (Huang et. al, 2022). JAK2 then phosphorylates (adds a phosphate group) to STAT3 (aka. stimulating phosphorylation and activating signal transducer and activator of transcription 3) to then initiate downstream signals. One of these signals includes transcribing the Socs3 gene (suppressors of cytokine signaling 3), which is a negative regulator of the JAK via feedback inhibition. What makes this pathway of particular interest is that, when inhibited, it blocks muscle wasting in cancer cachexia models when inhibited (Bonetto et. al, 2012, Rupert et al., 2021, Arneson-Wissink et al., 2024). Therefore, by taking into consideration both IL6 and phosphorylated STAT3 levels, we can better understand any correlations between the two in states of cachexia and the manner of signaling that IL6 may be engaging in.

There are two ways IL6 may interact with its receptor and engage in its signaling capacities: cis and trans. The major difference is where the receptor is located, either on the membrane of the cells via mbIL6-Rs as mentioned before, or in the plasma of the host as soluble IL6 receptor (sIL6-R), respectively. The main difference caused by trans-signaling is that when bound to the receptor, the IL6/IL6R complex can bind to any available membrane-bound gp130 subunits, which are present in every cell (Lacroix et. al, 2015). Therefore, actions that may not be regularly induced by IL6 on a specific cell could instead manifest, leading to other possible interactions. This is a point of interest as there could be

other potential mechanisms at this opens the field to a host of other target tissues that this complexed IL6 could be acting on to induce muscle wasting.

These signaling mechanisms play an important role in how IL6 one of its most notable effects: inflammation. Inflammation is a defense mechanism in which leukocytes, or white blood cells, migrate to the damaged tissue and destroy any potentially harmful factors that could induce even more tissue damage. The two types of inflammation are acute (severe and rapid onset) and chronic (mild and long-developing onset). IL6 is a major driver of acute inflammation, but can also act as an anti-inflammatory agent by producing the IL-1 receptor antagonist, an anti-inflammatory mediator. However, in chronic inflammation, IL6 is pro-inflammatory by exerting its effects on T and B cells. Its interactions with the soluble IL6 receptor have also been implicated in an integral factor for acute inflammation to develop into chronic inflammation (Gabay, 2006). While being a cytokine, IL6 can also influence multiple aspects of metabolism including glycolysis, oxidative phosphorylation, and fatty acid oxidation. It's been found to be significantly increased in viral diseases pertaining and is positively correlated to disease severity in cases of HPV or COPD which are often accompanied by significant weight loss (Li et. al, 2022).

In states of inflammation, IL6 is primarily produced by the liver and immune cells. In a pancreatic cancer environment, immune cells and fibroblasts in the cancer tumor microenvironment produce the most IL6 (Arneson-Wissink et. al, 2024; (Öhlund et. al, 2017). It has also been documented to affect gut and liver tissues via gastric homeostasis and liver regeneration and metabolism respectively (Schmidt-Arras et. al, 2015). However, if there is too much IL6 (i.e. as observed in research with mice models undergoing

prolonged, exercise), too much of the circulating IL6 (plasma IL6) from the skeletal muscle can cause muscle atrophy and wasting away (Haddad et. al, 2005).

However, one caveat is that the methods that IL6 takes specifically in cancer cachectic settings are yet to be determined, and if there are any other cofactors or secondary mechanisms involved in the signaling process related to progressing cancer cachexia. Research, particularly by Rupert et. al, has shown the most evidence that IL6 causes PDAC-associated cachexia and IL6 acts directly on the muscle. They noted that deleting IL6 from tumors improved PDAC-induced cachexia and mortality rates and that IL6-KO mice were entirely resistant to any muscle wasting. They found there is most likely a feed-forward signaling loop between tumor-derived IL6 that involves a potential trans-signaling mechanism in skeletal muscle which could induce both skeletal muscle and adipose wasting (Rupert et. al, 2021). Therefore, while speculated to be trans-signaling, the exact mechanism that IL6 takes is still unknown.

HYPOTHESIS & THESIS REASONING

Therefore, with all factors of current knowledge and research taken into consideration, we believe some connection between IL6, cancer cachexia, PDAC can be studied to study the onset of cancer cachexia and ultimately how to treat it. Evidence of both chronic inflammation and severely damaged metabolic processes, alongside prior research, show IL6 to be a target of promise in better understanding and therefore treating cachexia. There exists a plethora of evidence that suggests that IL6 plays a fundamental role in cachexia, but whether IL6 completes this by acting directly on skeletal muscle to induce wasting is still unknown. Therefore, we aim to elucidate the specific mechanism IL6 takes to induce cancer cachexia in a variety of models so that we can answer specific questions about necessity and sufficiency. This will also be done by looking at physical and biochemical factors to gain varied, corroborating data.

We hypothesize that in PDAC-associated models, IL6 is sufficient and necessary to induce muscle wasting by acting directly on skeletal muscle.

MATERIALS & METHODS

IL6/IL6-R ELISA Assay

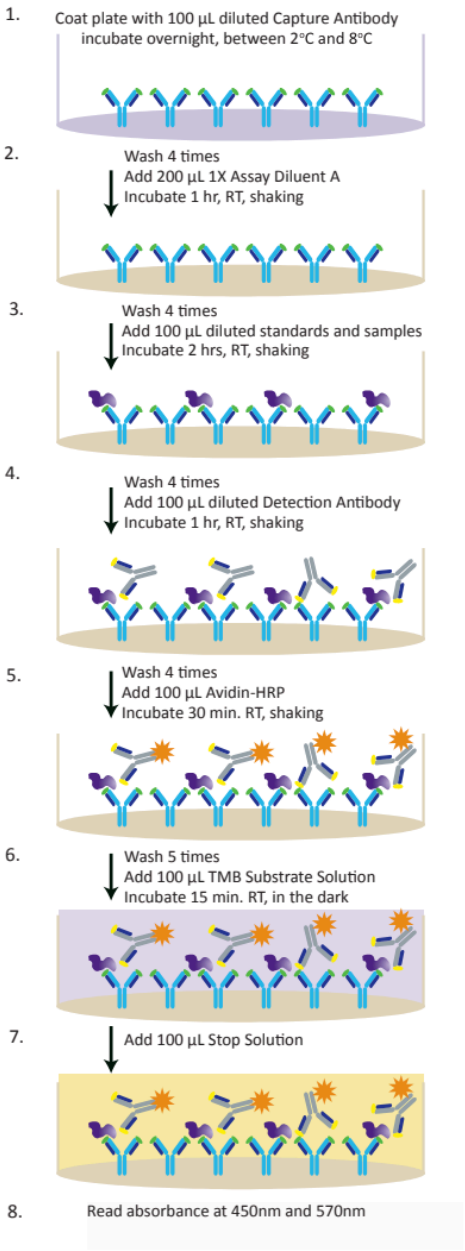

Diagram 1: IL6-ELISA (Sandwich) Assay Diagram.

A model of the general mechanics behind the assay used for this specific experimentation. *(Biolegend, 2019)*

An ELISA (enzyme-linked immunosorbent assay) is a common laboratory technique meant to detect certain proteins, hormones, antibodies, and antigens from bodily fluid samples such as blood or plasma. In our case, we employ both an IL6 and IL6-R ELISA to record the concentration of IL6 and IL6-R in the plasma of the mice implanted with PDAC tumors. This kind of ELISA assay is what's known as a "sandwich assay" as all of the components build and attach on top of one another. In our specific experimentation, the other follows as such, from bottom of the plate to the top: capture antibody, sample, detection antibody, and Avidin-HRP. Only in this order will they be able to interact properly and produce any result.

Some important reagents/materials are as follows:

- Coating Buffer: This stabilizes the antigen or antibody which is used to coat the ELISA plate, maximize adsorption to the plate, and optimize interactions with the detection antibody.
- Assay Diluent: This helps to equalize the antibody-binding efficiencies between the standard curve and the sample wells.
- Stop Solution: This stabilizes the color change of the medium, allowing a period in which the optical density of the assay can be accurately measured.
- Substrate Solution: This helps visualize and measure the color or signal generated during the ELISA reaction.
- PBS/Tween: A mild detergent will wash away those non-specific interactions.
- Detection Antibody: This detects a target antigen using highly specific antibody-antigen interactions.
- Avidin-HRP (Av-HRP): This is useful for detecting biotinylated antibodies

First, the 96-well plate is coated with the IL6 capture antibody via a coating buffer and sealed and incubated overnight at 4 degrees Celsius to ensure the antibody sticks securely to the well. Next, the unbound capture antibody is discarded by bringing the plate to room temperature and flicking off the capture antibody solution by hitting the plate against a hard surface. The plate is then washed thrice with PBS/Tween and any non-specific binding sites are blocked by adding 200 uL of Blocking Solution to each well. The plate is then sealed at room temperature and incubated for an hour, and the wash step is repeated once again (three times with PBS/Tween). Finally, the plate is blotted on top of a clean paper towel to empty the wells.

Standards and were then developed at the following concentrations, in the units pg/mL: 25, 125, 250, 500, 750, 1000, 1500, 2000. This process generates a standard curve to correlate plate absorbance to analyte concentration. The samples were diluted in Assay Diluent to arrive at the appropriate concentration and calculated binding efficiency. From there, the plates were sealed and incubated at 4 degrees Celsius overnight and then washed 3 times with PBS/Tween with additional flicking steps to ensure the wash was effective in removing any erroneous interactions.

The detection antibody that came with the associated BioLegend ELISA Assay kit (i.e. the respective ones for IL6 and IL6-R) was diluted to 0.25 ug/mL in Assay Diluent, and 100 uL of this diluted detection antibody was added to each well. The plate then followed the repeated process of being sealed and incubated for an hour and then washed three times with PBS/Tween. Av-HRP was then diluted to a 1:500 concentration, and 100 uL of each was added to each well. Once again, the plate was sealed and incubated for an hour, but this time washed five times with PBS/Tween.

Finally, the TMB Substrate Solution was prepared by mixing 6 mL each of TMB Reagent A and B, and 100 uL was transferred into each well. The plate was incubated at room temperature for 30 minutes for color development. The color reaction was then stopped by adding 100 uL of the Stop Solution to each well. Finally, the topical density was read at both 450 and 570 nm.

Tumor Implantation, Muscle Harvesting, & Mass Quantification in WT & IL6-KO Mice Models

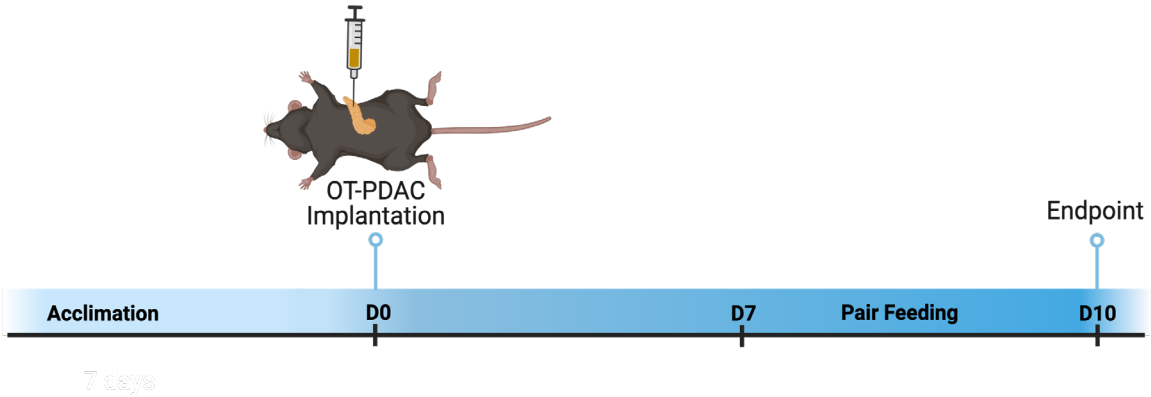

Diagram 2: Tumor Implantation, Muscle Harvesting & Mass Quantification in WT & IL6-KO Mice Models

A model of the general mechanics behind the implantation, harvesting, and quantification of skeletal muscle used for this specific experimentation. *(Bhaskar, 2022)*

Materials/Reagents:

- C57BL/6 mice: Wildtype (WT) mice are a common and widely used inbred strain of laboratory mice. They are very reliable as they exhibit a high uniformity in inherited characteristics and responses to experimental treatments. To maintain this genetic uniformity, the IGS, or the International Genetic Standardization Program, developed a pyramid mating system (Jackson Laboratory).

- IL6-knockout mice: IL6-KO mice, Another common strain of laboratory mice meant to explore the effects of the cytokine IL6 in the body, like responding to inflammation. These mice are null for the IL6 gene in all cells in the body, therefore making IL6 under any condition. They are viable and generally healthy, although are more susceptible to infection than WT mice. We are particularly interested in IL6-KO mice models as they have been known to recover from PDAC-associated cancer cachexia via decreasing tumor size and gaining of skeletal muscle mass. Therefore, we applied this model to study the influence of tumor-derived IL6 specifically. These mice were all purchased from Jackson Laboratories (Bar Harbor, ME).
- KPC cells: A well-established, reliable, and clinically relevant model of PDAC as it develops many features and symptoms that are present in human PDAC cases, one of them being cachexia (source). KPC stands for Kras, p53, and Cre: Kras and p53 are found to be two genes often mutated in human pancreatic tumors, while Cre is the genetic tool employed to control the activation/expression of the two genes. These cells were derived by taking a spontaneous pancreatic tumor from a KPC mouse and culturing the cancer cells. In our research, we have employed two lines of KPC cells – one known as "parental" (KPC – parental) that doesn't release any IL6 and another that overexpresses IL6 (KPC – IL6 OE).

First, mice were anesthetized with isoflurane and placed supine and the abdomen was then scrubbed with betadine. A para-midline incision was made in the left upper quadrant of the abdomen, cutting the muscle, and leaving the pancreas exposed. From there, mice either received 1,000,000 cells/23 uL of KPC - parental cells or KPC – IL6 OE cells to develop into their respective PDAC tumors or 23 uL of PBS via injections into the

pancreatic parenchyma. The pancreas was placed back into position so that the muscle cell was closed via 2 x sutures (4-0 polysorbate), and the skin was finally closed with 2 skin staples. It is worth noting that the implantation of the KPC cells directly into the pancreas to generate the PDAC tumor is known as an orthotopic implantation/tumor. On day 7, the mice then underwent the process of pair feeding, which involved restricting the food intake of the sham/control group to match that of the experimental group so that any difference due to food intake could be eliminated.

Finally, on day 10, the mice were terminated under isoflurane inhaled anesthesia, and the gastrocnemius (gastroc), tibialis anterior (TA), and plasma were collected accordingly. Specifically, the mass of the gastroc was recorded and then normalized to the mass of the gastroc at day 0 for further measurements. The biological samples were stored at -80 degrees C until further use.

Myofiber/Myotube IF-Staining

The general methodology of immunofluorescence staining the tissue samples for both anti-laminin and DAPI staining is the same, just with their respective antibodies. Therefore, they will both be outlined here.

Important Reagents/Materials:

- Anti-laminin antibody: Fluoresces green, a reliable marker of basement membranes surrounding blood vessels.
- DAPI: Fluoresces red, a reliable marker for nuclear DNA in both living and fixed cells.

TA samples from mice were thawed from storage on ice. Then, it follows the step of fixation with paraffin-formalin, dehydration with ethanol, embedded using paraffin wax,

and sectioned via microtone to an approximate 4-5 um thickness, placed on glass slides for microscopy use, and then stored at 4 degrees Celsius. When ready to be stained, the sections were first rimmed with a hydrophobic marker to ensure none of the fluids from the subsequent steps would leak over. First was the initial wash and permeabilization (i.e. puncturing the tissue membrane) to prepare the tissue sample thoroughly. This was done by transferring about 200-500 uL of PBS onto each sample twice for two minutes, PBS for 10 minutes, and then 0.25% PBS/gelatin/Triton twice for 10 minutes. Note after each wash, the solution was aspirated off, being careful not to aspirate the sample alongside it. The blocking step proceeded using 200uL of 5% BSA for each sample for about 60 minutes at room temperature. This prevented antibodies from binding to any non-target structures/factors present. Wet paper towels were lined inside the case containing the slides and the lid was enclosed to emulate a dark, humid environment.

Afterward, the BSA was aspirated, and 200 uL of either the respective DAPI or anti-laminin antibodies were added for each sample, and then incubated once again overnight, in its same dark and humid setting at room temperature to ensure that the primary antibody binds to the tissue appropriately. The following day, plates were washed with two PBS and one 0.25% PBS/gelatin/Triton washes for 10 minutes each in that order. The secondary antibody for anti-laminin staining was added to each sample at approximately 200 uL. This antibody was incubated for 60 minutes, in the same dark and humid box, at room temperature. Finally, the last set of washes occurs using PBS three times for 10 minutes, 10 nM $CuSO_4$ for 10 minutes, and then finally a quick rinse of dH_2O. The slides are then removed from the box and left to dry on a clean paper towel. Once ready to be mounted, a small drop of the mounting gel is placed onto the sample (already on the glass

microscopy slide) and then covered with a coverslip, ensuring there are no air bubbles via forceps, to ensure the sample is maintained properly. The slides are then kept in this horizontal position for drying in the dark for 24 hours RT, and then stored at 4 degrees Celsius.

From there, the samples are imaged via IF-microscope, and min feret diameters are quantified using ImageJ software (NIH, Bethesda, MD).

Conditioned Media Collection

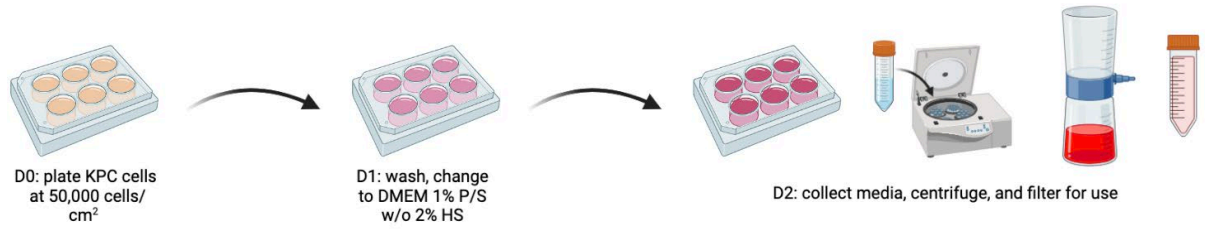

Diagram 3: Conditioned Media Collection Process

A model of the general mechanics behind the implantation, harvesting, and quantification of skeletal muscle used for this specific experimentation. *(Bhaskar, 2022)*

To develop the KPC – parental and KPC – IL6 OE conditioned media (CM), KPC parental or IL6 - OE cells respectively were plated at 500,00 cells/well using DMEM + 2% HS + 1% p/s for 24 hours. The following day, the media was aspirated, the cells were washed with PBS, and the media was changed to DMEM + 1% p/s without 2% HS. After 24 hours, the media was collected, centrifuged, filtered, and stored for later use at 4 degrees Celsius.

C2C12 Myotube Treatment

Important Reagents/Materials:

- Hyper IL6 (hIL6) stock: Solution of the IL6 + soluble IL6 receptor complex

- Recombinant murine IL6 (rIL6) stock: Solution of pure murine IL6

C2C12s were plated 300,000 cells/well, differentiated at day 1 and day 4 as per the "C2C12 Myotube Differentiation Procedure". Upon the second differentiation, cells were imaged, and specific treatments were started for the experimental groups. The control group was treated with DMEM media + 2%HS + 1%p/s, at 2 ml/well. For the rIL6 treatment group, cells were treated with DMEM media + 2%HS + 1%p/s + rIL6 (1uL rIL6 from 0.2mg/mL stock) at 2 mL/well. The hIL6 group was treated with DMEM media + 2%HS + 1%p/s + hIL6 (3.5 uL hyperIL6 200 ug/mL stock) at 2 mL/well. As per the conditioned media collection procedure, C2C12s were treated with KPC – parental and KPC – IL6 OE CM as per their respective experimental groups.

C2C12 Myotube Differentiation Procedure & Bright-field/IF-imaging

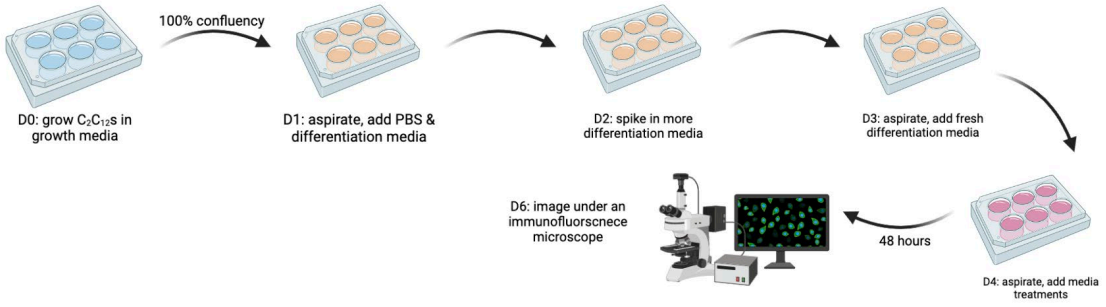

Diagram 4: Myotube Differentiation, IF-Staining, and Imaging Diagram.

A model of the general mechanics behind the assay used for this specific experimentation. *(Bhaskar, 2022)*

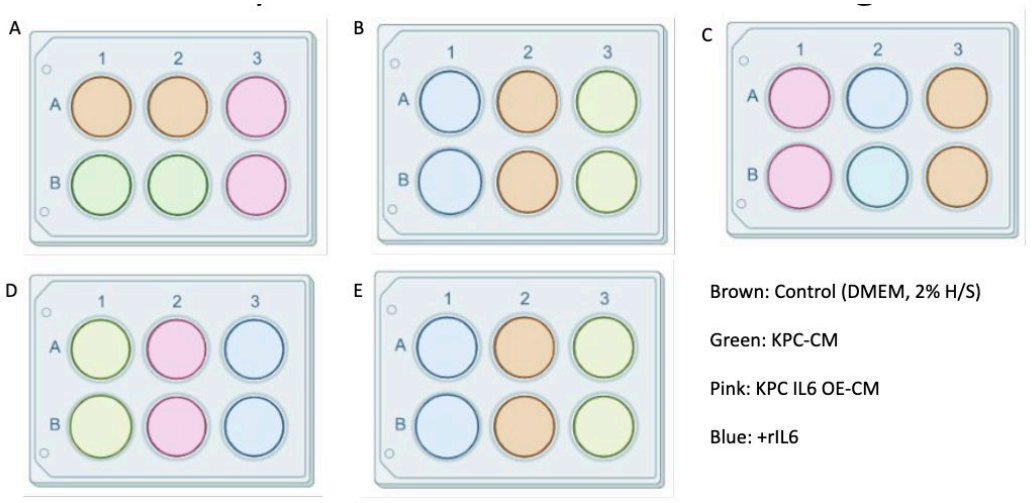

Diagram 5: Myotube Differentiation, IF-Staining, and Imaging Diagram.

A model of the general mechanics behind the assay used for this specific experimentation. *(Bhaskar, 2022)*

Each of the following steps (i.e. per step, as seen in the diagram) occurred for 24 hours

Important Reagents/Materials:

- C2C12 Myotubes: A reliable mouse myoblast cell line that forms contractile myotubes and produces characteristic muscle proteins.

C2C12s were plated at 300,00 cells/well and grown in growth media (DMEM high glucose, 10% FBS, 1% p/s). The media was then aspirated, washed with about 1 mL of PBS, and grown in differentiation media (DMEM high glucose, 2% HS, 1% p/s). More of the same differentiation media was spiked in and C2C12s were allowed to grow and differentiate. The old differentiation media was washed off and replaced with fresh differentiation media. Finally, the media was aspirated, and the experimental media treatments were added.

Brightfield images were taken at 0-hour and 48-hour time points, while IF images were taken after 48 hours. Only C2C12s treated with KPC – parental, KPC – IL6 OE, and rIL6

treatments (see the "C2C12 Myotube Treatment" section for rIL6 treatment components) were imaged, Diagram 4 portrays their respective layouts.

Myotube Diameter/Min Feret. Measuring & Quantification

Myotube diameters were measured using specific calibrations and tools on MyoVision software (Lexington, KY). For the four experimental treatments, when plated in cell culture plates, each well had three images taken and each image had 15 separate myotube diameter measurements.

Western Blotting & Measuring Relative Intensity

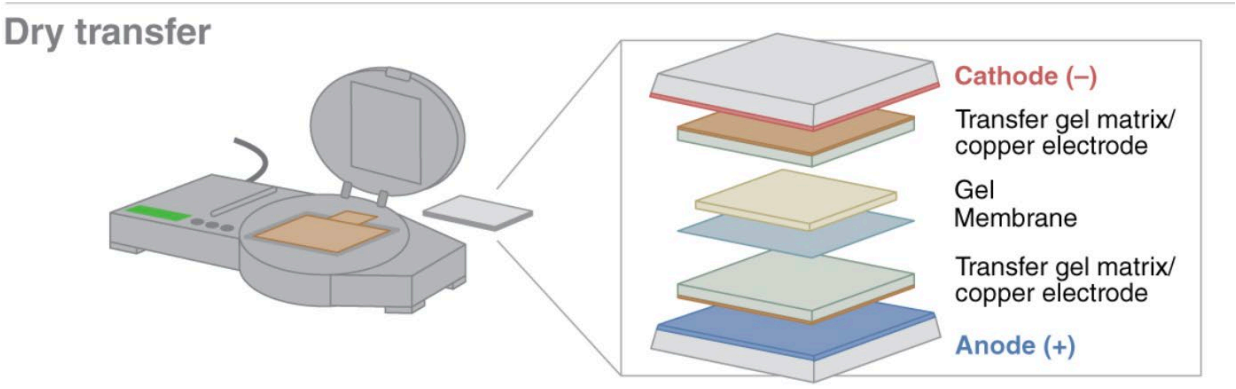

Diagram 6: Dry Transfer Protocols

A diagram of the dry transfer ordering of components for the western blot procedures. *(Kelesoglu, 2022)*

This process can be broken down into multiple steps: running the gel, dry transferring, protein transfer confirmation, blocking, adding antibodies, and imaging/quantifying. The dry transfer is specifically for transferring the proteins run from the gel to the membrane.

Important Reagents/Materials

- Running Buffer: Contains the appropriate ions that conduct current through the gel, separating proteins and drawing them through the matrix slab
- Transfer Buffer: Moves separated proteins from a gel to a solid support (i.e. the membrane)
- Blocking Agent: Prevents antibodies from binding to the membrane nonspecifically.

Firstly, the gel associated with the Novex WedgeWell kit was removed and washed with Tris-Glycine Running Buffer and placed into the appropriate gel apparatus. The gel chamber was then filled to the top with the running buffer and checked for air bubbles, while the lower chamber was filled to 2/3 of the same buffer. The protein samples to be loaded were first heated for 2 mins at 85 C and then loaded into the gel. The gel ran for 2-3 hours at about 90-100 V at around a current between 25-1 mA. Once complete and the gel was ready to be wet transferred, the appropriate wet membrane was prepped by being soaked in 100% methanol for 1 minute and then placed in a transfer buffer.

The gel was then transferred to the membrane and then assembled as seen in Diagram 6 under "Dry Transfer" alongside the other components. Note that both transfer stacks were soaked in 100% methanol for 2-3 minutes, and then placed in the associated Transfer Buffer from the Bio-Rad Turbo-Transfer kit. The transfer was initiated as per machine instructions, and once completed, the membrane was washed for 5 minutes in 1x TBS. To then check for protein transfer, the membrane was washed 2x for 2 min in ddH2O, stained in Ponceau stain for 4 minutes, imaged, and then finally de-stained with more ddH2O washes and washed completely with 1x TBS.

The membrane was then blocked via the respective blocking agent from the kit, and then incubated with the respective primary and secondary antibodies for STAT3 and pSTAT3. Each antibody was incubated for about an hour each, in dark conditions at room temperature to ensure proper binding. Finally, the membrane was imaged via Odyssey software.

RT-qPCR

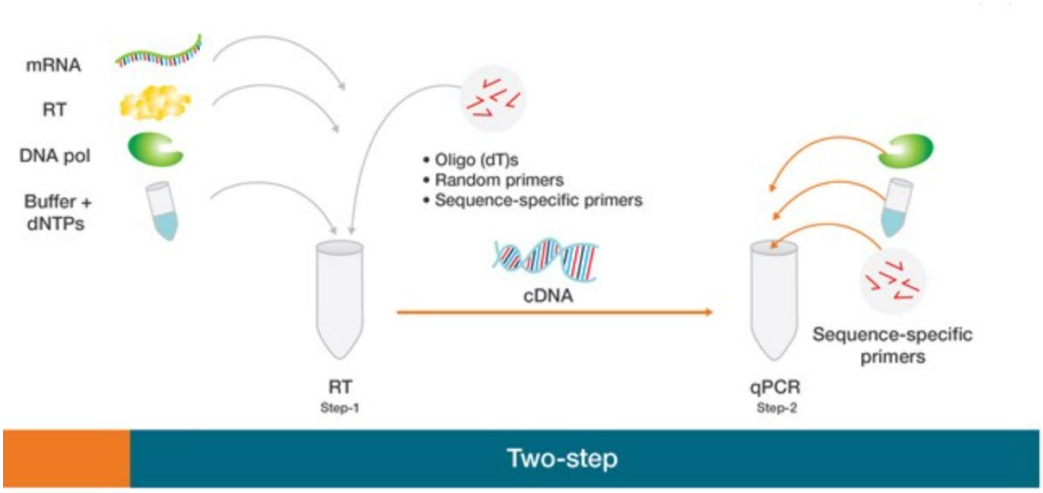

Diagram 7: RT-qPCR Outline

Overview of the steps and components of an RT-qPCR protocol, *("Basic")*

This procedure can be broken down into two steps, the reverse transcription, and the actual PCR. This first step creates the cDNA we are studying, and the second step amplifies the specific portion of the DNA we want to study.

Important Reagents/Materials

- Random Decamers: Primes single-stranded DNA or RNA for extension by DNA polymerases or reverse transcriptase.

- dNTP mix: Provides single bases ready to go into DNA and double it, like building blocks.
- Reverse Transcriptase: Concerts RNA to DNA

The first step uses a combination of about 2 uL of RNA sample, 2 uL of random decamers, 2 uL of 10X RT Buffer, 4 uL of dNTP mix, 1 uL of RNase inhibitor, 1 uL of reverse transcriptase, and 8 uL of nuclease-free water. This combined is gently spun, and then incubated at 44 C for an hour and then at 92 C for 10 minutes to inactivate the reverse transcriptase. Upon completion, the PCR is completed by combining 2 uL of the cDNA from the prior reaction, 2.5 uL of 10X PCR Buffer, 1.25 uL of forward primer, 1.25 uL of reverse primer, 1.25 uL of dNTP mix, 0.2 uL of Taq Polymerase, and a remaining 17.5 uL of ddH2O. This is then incubated at 94 C for 4 minutes for the initial denaturation of the cDNA, and then 30 cycles of denaturation at 94 C for 30 seconds, annealation at 55 C for 30 seconds, and extension at 72 C for 45 seconds, and then a final extension at 72 C for 5 minutes. The following concentrations were then measured via fluorescent measurements per cycle to account for relative quantification.

Statistical Analysis

All statistical analysis was conducted via one-way ANOVAs, with a significance set at $p < 0.5$. Any pairwise comparisons were conducted using t-tests. Both the statistical and graphing software was GraphPad Prism, version 10.

RESULTS & FIGURES

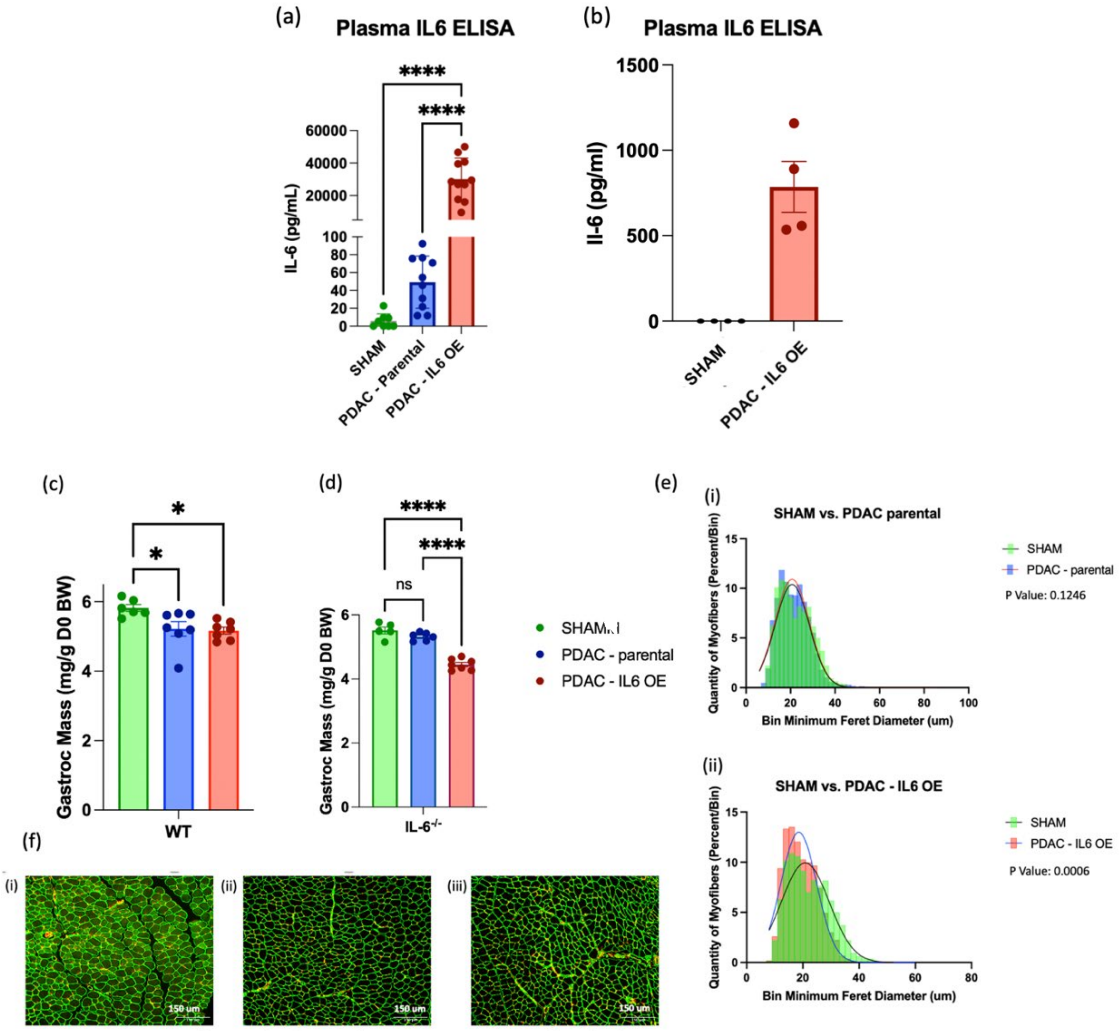

Figure 1: Tumor-derived IL6 leads to loss in skeletal muscle mass

(a) Plasma IL6 concentrations in wild-type (WT) mice implanted with experimental PDAC tumors orthotopically (OT), measured at day 5. (b) Plasma IL6 concentration in IL6-knock out (IL6-KO) mice implanted with PDAC – IL6 OE tumors orthotopically measured at day 5. (c) Gastrocnemius (gastroc) mass measured WT and (d) IL6-KO mice implanted with experimental PDAC tumors orthotopically were measured at day 10. (e) Minimum feret quantification of tibialis anterior (TA) muscle myofibers (um) of (i) PDAC - parental and (ii) PDAC - IL6 OE implanted IL6-KO mice compared to SHAM IL6-KO mice. Histogram fitted with nonlinear regression. (f) IF-stained images of TA muscle from (i) SHAM, (ii) PDAC-parental, and (iii) PDAC-IL6 OE implanted IL6-KO mice. Fluorescent green: anti-laminin staining. Fluorescent red: DAPI staining.

1.1: Tumor-derived IL6 in PDAC models is sufficient to drive skeletal muscle mass loss

In prior research, our lab showed that IL6-KO mice are resistant to cachexia. We were first interested in whether reinstating IL6 expression in PDAC-bearing IL6-KO mice can restore cachexia/muscle wasting. We generated a specific PDAC tumor type using cancer cells derived from the *KrasG12D/+*; *Tp53R172H/+*; *Pdx-cre* (KPC) that overexpressed in IL6. Orthotopic PDAC mice models were created by implanting these PDAC – IL6 OE tumors and PDAC - parental tumors into the pancreatic tail (Michaelis et. al, 2017) of both WT and IL6-KO mice. We saw elevated IL6 concentrations in WT mice implanted with PDAC – parental and PDAC – IL6 OE tumors, with the most increase in IL6 levels in the PDAC – IL6 OE tumors models compared to the other two groups (Figure 1a). In the IL6-KO mice, we measured IL6 concentrations from PDAC IL6 – OE tumors and found an increase (Figure 1c). Prior work from our lab showed that the PDAC – parental cells do not produce IL6 and no IL6 was detected when these cells were implanted in IL6-KO mice (Arneson-Wissink et al., 2024).

With the model established, we wanted to determine whether reintroducing IL6 in tumor-bearing IL6KO mice was sufficient to induce skeletal muscle mass wasting. We measured the skeletal muscle mass (Figure 1e) and myofiber size (via min ferret diameter quantifications using Fiji) in those same models on day 10 after tumor implantation (Figure 1f). In WT mice, we found that both the PDAC – parental and PDAC IL6 – OE tumors induced significant muscle wasting, as measured by a decrease in gastric mass. IL6-KO mice were resistant to muscle wasting induced by the PDAC – parental cells, as measured by both gastroc mass and TA myofiber diameter. Reintroducing IL6 in tumor-bearing IL6KO mice was sufficient to induce muscle wasting, causing decreases in gastroc mass and TA myofiber diameter (Figure 1c-f).

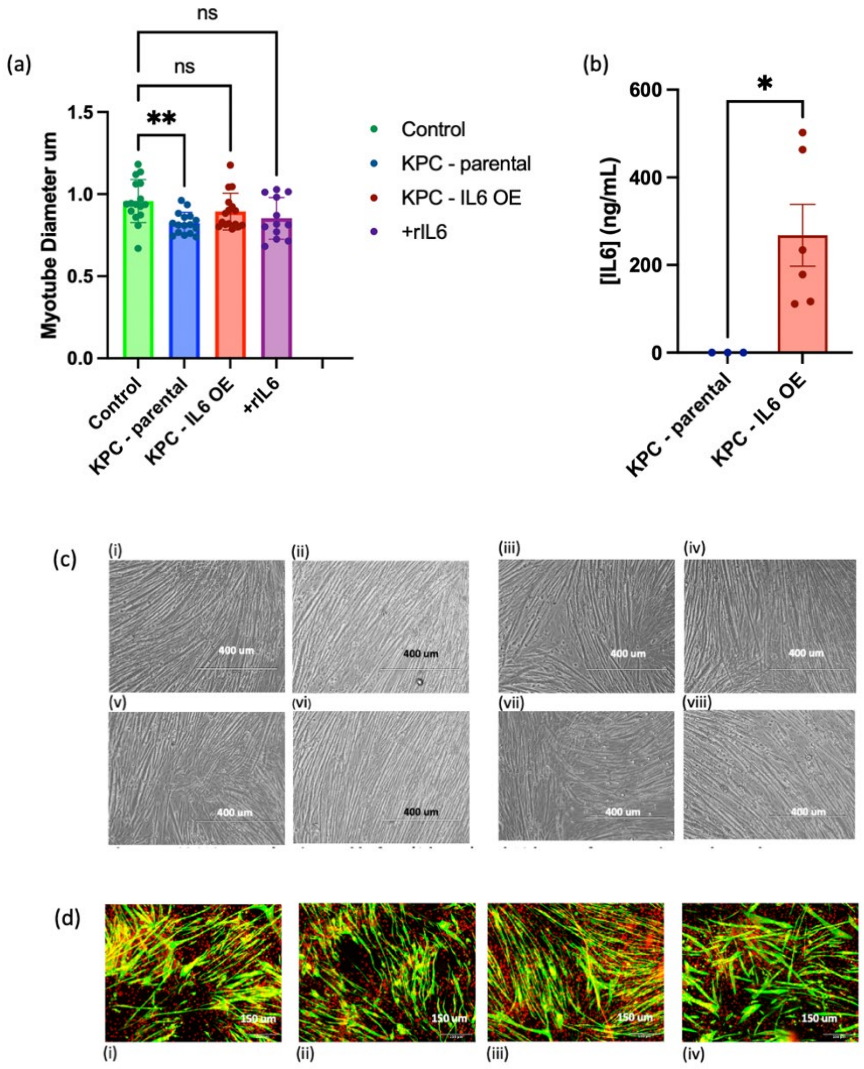

Figure 2: C2C12 myotube atrophy quantification by myotube diameter

(a) Myotube diameter of C2C12s (um) treated with control, KPC - parental CM, KPC - IL6 OE CM, and +rIL6 treatments. (b) IL6 concentration in the KPC – parental CM and KPC – IL6 OE CM. (c) Control C2C12 myotubes at (i) 0 hours and (ii) 48 hours. C2C12 myotubes at (iii) 0 hours pre-KPC – parental CM treatment and (iv) 48 hours post-KPC - parental CM treatment. C2C12 myotubes at (v) 0 hours pre-KPC - IL6 OE CM treatment and (vi) 48 hours post-KPC - IL6 OE CM treatment. C2C12 myotubes at (vii) 0 hours pre recombinant IL6 (+rIL6, 20ng/mL) treatment and (viii) 48 hours post +rIL6 treatment. (d) Control, (ii) KPC – parental CM, (iii) KPC - IL6 OE CM, and (iv) +rIL6 treated C2C12 myotubes. Fluorescent green: anti-laminin staining. Fluorescent red: DAPI staining.

1.2: Parental KPC-conditioned media, but not IL6 OE-conditioned media causes atrophy of C2C12 myotubes *in vitro*

From our prior studies, we know that IL6 is both necessary and sufficient to induce wasting in mice bearing PDAC tumors. Knowing that cachexia is defined by enhanced skeletal muscle wasting, we wanted to determine whether IL6 acts directly on skeletal muscle to induce wasting. To do this, we developed an in vitro model of skeletal muscle wasting, using C2C12 myotubes and sought to validate this approach as a model of muscle wasting. To do so, we treated these cells with media that had been conditioned for 48 hours by either KPC - parental cells (without IL6), KPC - IL6 OE cells (with very high levels of IL6) or the addition of recombinant murine IL6 (rIL6) alone (Figure 2a). We also ran an IL6 ELISA to determine the exact concentrations of IL6 in the two conditioned media treatments (Figure 2b).

We found that, although the KPC – parental CM had no IL6 and the KPC – IL6 OE had a much higher concentration, the KPC – parental CM induced myofiber atrophy in C2C12. As a positive control for IL6 activity on the myotubes, we evaluated the phosphorylation of STAT3, an effector of IL6 signaling, and the expression of suppressor of cytokine signaling-3 (*Socs3*), which is induced by STAT3.

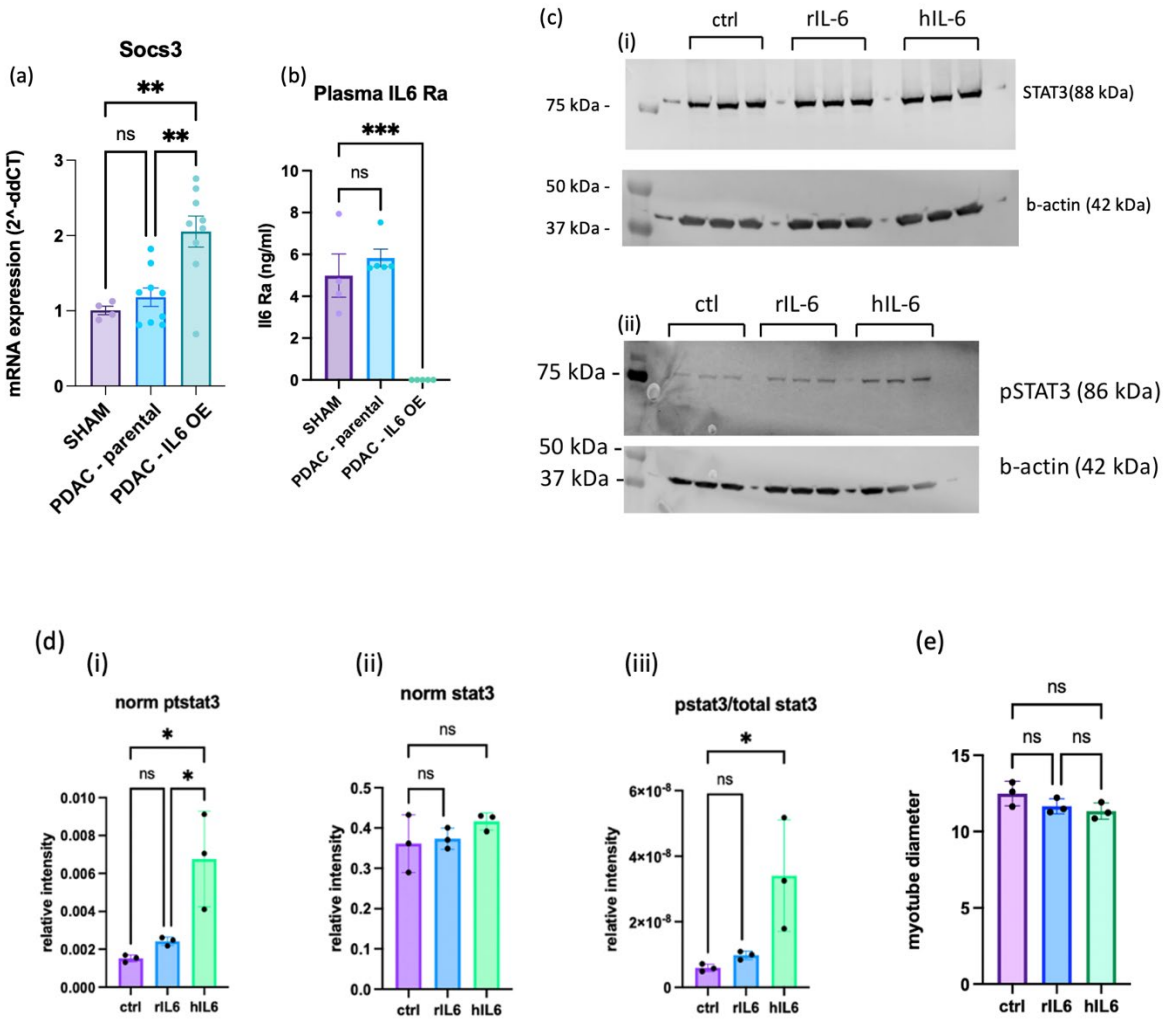

Figure 3: In vivo and in vitro observations of the indication of the IL6 signaling and muscle wasting.

(a) qPCR expression of Socs3 in WT mice implanted PDAC-parental or PDAC-IL6 OE tumors. (b) sIL6-R concentration in IL6-KO mice when implanted PDAC-parental or PDAC-IL6 OE tumors. (c) Western Blot of C2C12s treated with rIL6 and hIL6, measuring (i) STAT3 and (ii) pSTAT3 expression. (d) Relative intensity measurements of STAT3 pathway activation from (b) when C2C12s are treated with rIL6 or hIL6. (i) pSTAT3, (ii) STAT3, and (iii) normalized pSTAT3 values were measured and statistically analyzed. (e) Myotube diameter of C2C12 myotubes treated with rIL6 or hIL6

1.3: Socs3 is activated significantly when in the presence of hyper-IL6 in C2C12s and in IL6-KO mice implanted with PDAC-IL6 OE cells.

At this point, our in vitro data suggest that IL6 may not be sufficient to induce wasting via direct activity on skeletal myocytes. We considered that perhaps muscle wasting relies on IL6 trans-signaling, which occurs in multiple pathologic conditions. IL6 trans-signaling is when IL6 interacts with a soluble IL6 receptor (sIL6-R) which travels freely throughout the system, thereby making it potentially able to interact with all cell types, including those that don't express IL6-R. This is in comparison to IL6 cis-signaling, which is when IL6 only interacts with the membrane-bound IL6 receptor (mbIL6-R) that's only found on limited cell types, thereby making the subsequent actions of bound IL6 constrained to just those cells (Lacroix et. al, 2015).

In our prior in vitro study, there were no cells to provide the sIL6R required for trans signaling, so we wanted to compare cis- vs trans-IL6 signaling to see whether trans signaling is necessary for muscle wasting. We first looked in vivo at the expression of Socs3, which is a marker of elevated IL6 signaling, in IL6-KO mice challenged for 5 days. We found that only the IL6OE and not the parental tumors showed increased Socs3 in the skeletal muscle (Figure 3a). At this time point, IL6 levels are substantially higher in the IL - 6OE mice as well (Figure 1b). To then consider the possibility of trans-signaling, we conducted an sIL6-R ELISA in those same IL6-KO mice to determine the concentration of sIL6-R and found there was essentially none in the mice implanted with PDAC – IL6 OE tumors compared to the controls. With these data and the prior gastroc mass measurements (Figure 1d) and IL6 concentrations (Figure 1a), there is evidence that IL6 directly signals onto skeletal muscle, but that specific signaling is not necessary to induce muscle atrophy as the PDAC – parental tumor implanted in WT mice did not exhibit any wasting. (Figure 1d).

With that, we then wanted to answer the question if IL6 is sufficient in causing muscle wasting. We moved into an in vitro model using C2C12 myotubes to do so. An integral aspect of determining this is evaluating the activation of the IL6/JAK2/STAT3 pathway. We measured the activity of the IL6/JAK2/STAT3 pathway by quantifying phosphorylated STAT3 (pSTAT3) protein and Socs3 mRNA expression levels.

Therefore, we wanted to see if STAT3 could be activated (i.e., phosphorylated) with just rIL6 or hIL6 (hyper IL6, a complex of IL6 and sIL6R that mimics trans-signaling) and if myofiber atrophy. Upon western blotting (Figure 3b), we saw increased pSTAT3 with hIL6 but, not rIL6, suggesting that C2C12 myotubes do not express enough mbIL6-R to allow IL6 cis-signaling. We observed no significant myofiber atrophy in either IL6-treated condition. Therefore, while a hIL6 is sufficient to induce STAT3 activation, it is insufficient to induce myofiber atrophy.

DISCUSSION

This thesis aimed to study the effects of IL6 on muscle atrophy in PDAC models to determine whether the cytokine IL6 drives cancer-associated muscle wasting by acting directly on the muscle cells. Our studies investigated the effects of IL6 on muscle wasting in an orthotopic PDAC tumor mouse model in both WT and IL6-KO mice and in C2C12 cell culture. Muscle wasting was measured via skeletal muscle mass and myofiber atrophy, and IL6 signaling was then measured by recording levels of Socs3 and pSTAT3 expression. Our data show that (1) IL6 is both necessary and sufficient for muscle wasting in PDAC models, (2) IL6's catabolic actions are not due to direct signaling to muscle, and (3) while hIL6 is sufficient to activate the STAT3 pathway, it does not induce myofiber atrophy via direct muscle signaling.

I. IL6 is both necessary and sufficient for PDAC-associated muscle wasting in vivo.

Initial experiments evidenced that IL6-KO mice implanted with PDAC cells that overexpress IL6 had a significant loss in skeletal muscle mass, whereas those implanted with parental PDAC cells did not show muscle wasting. This is consistent with what we would have anticipated originally, as it has been cited to induce muscle wasting (Haddad et al.). Additionally, it has been previously noted in our lab's former research that IL6-KO mice are resistant to PDAC-induced muscle mass.

WT and IL6-KO mice implanted with the PDAC – IL6 OE cells both show a rise in plasma IL6 concentrations. Both WT and IL6-KO mice implanted with PDAC – IL6 OE tumors showed muscle wasting, but only WT, not IL6KO, showed wasting with parental cells. Therefore, by getting rid of all IL6 in the IL6-KO mouse, we could reverse muscle wasting caused by the parental cells—thus demonstrating that IL6 is necessary. By overexpressing IL6 in the tumor cells, muscle wasting was restored in IL6KO mice, demonstrating that IL6 is sufficient

to induce wasting. This indicates that IL6 is necessary and sufficient to induce skeletal muscle wasting. In other words, the tumor itself was insufficient on its own, but the addition of IL6 now permits wasting to occur.

II. IL6's catabolic actions are not due to direct signaling on skeletal myocytes.

When administered to C2C12 myotubes, rIL6 does not induce any myofiber atrophy or significant increase in STAT3 phosphorylation. This is indicative that cis-signaling is not occurring. Therefore, IL6 trans-signaling mechanisms were considered and explored as an alternate possibility. Prior research has linked IL6 trans-signaling to other cancers likes hepatocellular adenomas and carcinoma (Gyorffy et. al, 1989) to seemingly unrelated diseases in completely other areas of the body like periodontitis (Genco et. al, 2001). Additionally, tissue IL6 sensitivity can potentially increase via an IL6 trans-signaling cascade as mediated by sIL6-R. Since sIL6-R expression is in turn mediated by immune system players like neutrophils and macrophages, the trans-signaling pathway is heavily associated with the pro-inflammatory states of disease, states like cancer cachexia (Narsale et. al, 2015). Therefore, we studied any potential effects of trans-signaling by treating C2C12 myotubes with hIL6 – a complexed version of IL6 and sIL6-R. However, no significant myofiber atrophy was found with this treatment in comparison to those treated with rIL6 and the control, despite evidence of active IL6 signaling (increased Socs3 expression and STAT3 phosphorylation). Therefore, we conclude that IL6's catabolic actions are not due to direct signaling to the muscle.

Now that direct signaling to the muscle does not seem to be the answer, we can consider other indirect mechanisms that induce muscle wasting. For instance, Arnesson-Wissink et. al show that IL6 acts directly on the liver in PDAC to suppress beta-oxidation (the process of breaking down fatty acids into substrates for ATP production) and ketogenesis (the production of

ketone bodies due to breaking down fatty acids). They find that restoring ketogenesis either through feeding PDAC mice a ketogenic diet or by deleting STAT3 from hepatocytes can prevent muscle wasting. Their findings note that because of the undernutrition due to PDAC, dependence on lipid metabolism would be increased. Therefore, IL6-induced suppression of ketogenesis and beta-oxidation in cancer increases susceptibility to wasting.

Another possible example would be that IL6 induces adipose wasting, which in turn can enhance muscle wasting. A protein known as CIDEA has been with lipolysis and thermogenesis and is stimulated by IL6/STAT3 pathway activation and signaling. CIDEA levels positively correlate with free fatty acid plasma levels, which is a common indicator of lipolysis and weight loss. A lack of energy that can be associated with weight loss activates the adenosine monophosphate-activated protein kinase (AMPK), which promotes energy conservation. However, as a regulatory mechanism, CIDEA mediates AMPK degradation, which is a process that is essential for lipolysis that if at high enough rates, can induce cachexia in cancerous states (Radaványi et. al, 2024). This is a possible explanation for excessive fat catabolism, which other research has shown is often necessary for muscle catabolism to subsequently ensue. Prior research has shown that free fatty acids, the product of lipolysis, may directly attenuate the breakdown of myofibrillar proteins in states of prolonged starvation (Lowell et. al, 1987). Cancer cachexia is a state of prolonged starvation; therefore, this could be the potential actions that are occurring in these PDAC models that we may not be noticing from our experimentation alone.

III. While hIL6 activates STAT3, it does not induce myotube atrophy.

When comparing the activations of different conformations of IL6, hIL6 is the only condition that both increased Socs3 expression and activated the STAT3 pathway in our C2C12 model. This finding suggests that myotubes are incapable of responding fully to IL6 alone via

cis-signaling. One explanation for this would be that C2C12 myotubes do not express IL6R. We did not assess the mRNA or protein expression of IL6R in these cells, so this remains an open question. As noted previously, the STAT3 pathway can block muscle wasting in cancer cachexia models when inhibited. However, activation of STAT3 in muscle is not enough to induce any muscle atrophy, as observed by the lack of decrease in myofiber diameter in the C2C12s. This reaffirms the possibility the hIL6 form interacts with cofactors and molecules or on different tissues altogether in an *in vivo* setting to initiate muscle atrophy in a cachectic environment.

LIMITATIONS & FUTURE DIRECTIONS

Some limitations existed in our work that didn't allow us to create a full picture of what was happening. One such limitation is that we did not measure IL6R expression in C2C12 myotubes, so the reason rIL6 did not increase STAT3 phosphorylation is not clear. A second concern was that in our mouse models, we did not test whether IL6 acts directly on the muscle in vivo. In the future, we plan to do this by generating mice in which STAT3 is deleted only from skeletal myocytes, and then testing whether these mice are resistant to PDAC cachexia. We also did not assess the activation of catabolic pathways in muscle in either the in vivo or in vitro conditions to evaluate the relationship between IL6 activation of muscle STAT3 and known catabolic mediators. Another limitation is that we did not test the effects of IL6 signaling on adipose reserves, basal metabolic rate, or food intake in vivo, so the contributions of these pathways are purely speculative. Finally, these data only reflect a single cachexia model and a single mediator of cachexia and so may not be generalizable to other models or patients. We hope in future experiments to consider these factors when continuing our experimentation, while also taking into consideration the alternative mechanisms discussed prior.

CONCLUSION

Cancer cachexia is a state of severe undernutrition that leads to skeletal muscle wasting and is a common symptom faced by many PDAC patients. One of the main factors of cancer cachexia is a state of inflammation, such as that induced by IL6. We hypothesized that in PDAC-associated models, IL6 is sufficient and necessary to induce muscle wasting by acting directly on skeletal muscle. In our models of IL6-KO mice that were initially resistant to cachexia, we found that reinstating IL6 via PDAC tumors could induce cancer cachexia, thereby showing it was necessary and sufficient for cancer cachexia to present itself. However, when treating C2C12 myotubes with KPC CM and different conformations of IL6 (rIL6 and hIL6), we noted no myofiber atrophy in the presence of hIL6, despite activation of the relevant IL6/JAK2/STAT3 pathway. This indicates that IL6 does not act directly on skeletal muscle to induce its wasting but rather an indirect signaling mechanism instead.

BIBLIOGRAPHY

Ahlberg K, Ekman T, Gaston-Johansson F, Mock V. Assessment and management of cancer-related fatigue in adults. Lancet. 2003 Aug 23;362(9384):640-50. doi: 10.1016/S0140-6736(03)14186-4. PMID: 12944066.

Arneson-Wissink PC, Mendez H, Pelz K, Dickie J, Bartlett AQ, Worley BL, Krasnow SM, Eil R, Grossberg AJ. Hepatic signal transducer and activator of transcription-3 signaling drives early-stage pancreatic cancer cachexia via suppressed ketogenesis. J Cachexia Sarcopenia Muscle. 2024 Apr 17. doi: 10.1002/jcsm.13466. Epub ahead of print. PMID: 38632714.

Bonetto A, Aydogdu T, Jin X, Zhang Z, Zhan R, Puzis L, Koniaris LG, Zimmers TA. JAK/STAT3 pathway inhibition blocks skeletal muscle wasting downstream of IL6 and in experimental cancer cachexia. Am J Physiol Endocrinol Metab. 2012 Aug 1;303(3):E410-21. doi: 10.1152/ajpendo.00039.2012. Epub 2012 Jun 5. PMID: 22669242; PMCID: PMC3423125.

Bhaskar, Mayurika, “Figures & Diagrams”, 2022

BioLegend, 2019, www.biolegend.com/Files/Images/media_assets/pro_detail/datasheets/430504_V02.pdf.

Capasso M, Franceschi M, Rodriguez-Castro KI, Crafa P, Cambiè G, Miraglia C, Barchi A, Nouvenne A, Leandro G, Meschi T, De' Angelis GL, Di Mario F. Epidemiology and risk factors of pancreatic cancer. Acta Biomed. 2018 Dec 17;89(9-S):141-146. doi: 10.23750/abm.v89i9-S.7923. PMID: 30561407; PMCID: PMC6502190.

Fearon KC. Cancer cachexia: developing multimodal therapy for a multidimensional problem. Eur J Cancer. 2008 May;44(8):1124-32. doi: 10.1016/j.ejca.2008.02.033. Epub 2008 Mar 28. PMID: 18375115.

Fearon K, Strasser F, Anker SD, Bosaeus I, Bruera E, Fainsinger RL, Jatoi A, Loprinzi C, MacDonald N, Mantovani G, Davis M, Muscaritoli M, Ottery F, Radbruch L, Ravasco P, Walsh D, Wilcock A, Kaasa S, Baracos VE. Definition and classification of cancer cachexia: an international consensus. Lancet Oncol. 2011 May;12(5):489-95. doi: 10.1016/S1470-2045(10)70218-7. Epub 2011 Feb 4. PMID: 21296615.

Gabay C. Interleukin-6 and chronic inflammation. Arthritis Res Ther. 2006;8 Suppl 2(Suppl 2):S3. doi: 10.1186/ar1917. Epub 2006 Jul 28. PMID: 16899107; PMCID: PMC3226076.

Grossberg AJ, Chu LC, Deig CR, Fishman EK, Hwang WL, Maitra A, Marks DL, Mehta A, Nabavizadeh N, Simeone DM, Weekes CD, Thomas CR Jr. Multidisciplinary standards of care and recent progress in pancreatic ductal adenocarcinoma. CA Cancer J Clin. 2020

Sep;70(5):375-403. doi: 10.3322/caac.21626. Epub 2020 Jul 19. PMID: 32683683; PMCID: PMC7722002.

Haddad F, Zaldivar F, Cooper DM, Adams GR. IL6-induced skeletal muscle atrophy. J Appl Physiol (1985). 2005 Mar;98(3):911-7. doi: 10.1152/japplphysiol.01026.2004. Epub 2004 Nov 12. PMID: 15542570.

Hopkinson J. Psychosocial Support in Cancer Cachexia Syndrome: The Evidence for Supported Self-Management of Eating Problems during Radiotherapy or Chemotherapy Treatment. Asia Pac J Oncol Nurs. 2018 Oct-Dec;5(4):358-368. doi: 10.4103/apjon.apjon_12_18. PMID: 30271817; PMCID: PMC6103201.

Huang B, Lang X, Li X. The role of IL6/JAK2/STAT3 signaling pathway in cancers. Front Oncol. 2022 Dec 16;12:1023177. doi: 10.3389/fonc.2022.1023177. PMID: 36591515; PMCID: PMC9800921.

Kelesoglu, Nicole. "The Pros and Cons of Wet, Semi-Dry and Dry Transfer for Western Blots Labconscious®." *Labconscious*®, Labconscious®, 21 Nov. 2022, www.labconscious.com/green-lab-tips/the-pros-and-cons-of-wet-semi-dry-and-dry-transfer-for-western-blots.

Li YS, Ren HC, Cao JH. Roles of Interleukin-6-mediated immunometabolic reprogramming in COVID-19 and other viral infection-associated diseases. Int Immunopharmacol. 2022 Sep;110:109005. doi: 10.1016/j.intimp.2022.109005. Epub 2022 Jun 28. PMID: 35780641; PMCID: PMC9236983.

Michaelis KA, Zhu X, Burfeind KG, Krasnow SM, Levasseur PR, Morgan TK, Marks DL. Establishment and characterization of a novel murine model of pancreatic cancer cachexia. J Cachexia Sarcopenia Muscle. 2017 Oct;8(5):824-838. doi: 10.1002/jcsm.12225. Epub 2017 Jul 20. PMID: 28730707; PMCID: PMC5659050.

Öhlund D, Handly-Santana A, Biffi G, Elyada E, Almeida AS, Ponz-Sarvise M, Corbo V, Oni TE, Hearn SA, Lee EJ, Chio II, Hwang CI, Tiriac H, Baker LA, Engle DD, Feig C, Kultti A, Egeblad M, Fearon DT, Crawford JM, Clevers H, Park Y, Tuveson DA. Distinct populations of inflammatory fibroblasts and myofibroblasts in pancreatic cancer. J Exp Med. 2017 Mar 6;214(3):579-596. doi: 10.1084/jem.20162024. Epub 2017 Feb 23. PMID: 28232471; PMCID: PMC5339682.

Orth M, Metzger P, Gerum S, Mayerle J, Schneider G, Belka C, Schnurr M, Lauber K. Pancreatic ductal adenocarcinoma: biological hallmarks, current status, and future perspectives of combined modality treatment approaches. Radiat Oncol. 2019 Aug 8;14(1):141. doi: 10.1186/s13014-019-1345-6. PMID: 31395068; PMCID: PMC6688256.

Pereira SP, Oldfield L, Ney A, Hart PA, Keane MG, Pandol SJ, Li D, Greenhalf W, Jeon CY, Koay EJ, Almario CV, Halloran C, Lennon AM, Costello E. Early detection of pancreatic cancer. Lancet Gastroenterol Hepatol. 2020 Jul;5(7):698-710. doi: 10.1016/S2468-1253(19)30416-9. Epub 2020 Mar 2. PMID: 32135127; PMCID: PMC7380506.

Porta M, Fabregat X, Malats N, Guarner L, Carrato A, de Miguel A, Ruiz L, Jariod M, Costafreda S, Coll S, Alguacil J, Corominas JM, Solà R, Salas A, Real FX. Exocrine pancreatic cancer: symptoms at presentation and their relation to tumour site and stage. Clin Transl Oncol. 2005 Jun;7(5):189-97. doi: 10.1007/BF02712816. PMID: 15960930.

Poulia KA, Sarantis P, Antoniadou D, Koustas E, Papadimitropoulou A, Papavassiliou AG, Karamouzis MV. Pancreatic Cancer and Cachexia-Metabolic Mechanisms and Novel Insights. Nutrients. 2020 May 26;12(6):1543. doi: 10.3390/nu12061543. PMID: 32466362; PMCID: PMC7352917.

Rahib L, Smith BD, Aizenberg R, Rosenzweig AB, Fleshman JM, Matrisian LM. Projecting cancer incidence and deaths to 2030: the unexpected burden of thyroid, liver, and pancreas cancers in the United States. Cancer Res. 2014 Jun 1;74(11):2913-21. doi: 10.1158/0008-5472.CAN-14-0155. Erratum in: Cancer Res. 2014 Jul 15;74(14):4006. PMID: 24840647.

Radványi Á, Röszer T. Interleukin-6: An Under-Appreciated Inducer of Thermogenic Adipocyte Differentiation. Int J Mol Sci. 2024 Feb 28;25(5):2810. doi: 10.3390/ijms25052810. PMID: 38474057; PMCID: PMC10932467.

Rupert JE, Narasimhan A, Jengelley DHA, Jiang Y, Liu J, Au E, Silverman LM, Sandusky G, Bonetto A, Cao S, Lu X, O'Connell TM, Liu Y, Koniaris LG, Zimmers TA. Tumor-derived IL6 and trans-signaling among tumor, fat, and muscle mediate pancreatic cancer cachexia. J Exp Med. 2021 Jun 7;218(6):e20190450. doi: 10.1084/jem.20190450. PMID: 33851955; PMCID: PMC8185651.

Schmidt-Arras D, Rose-John S. IL6 pathway in the liver: From physiopathology to therapy. J Hepatol. 2016 Jun;64(6):1403-15. doi: 10.1016/j.jhep.2016.02.004. Epub 2016 Feb 8. PMID: 26867490.

Siegel, R. L., Giaquinto, A. N., & Jemal, A. (2024). Cancer statistics, 2024. *CA: A Cancer Journal for Clinicians*, *74*(1), 12-49. https://doi.org/10.3322/caac.21820

Simpson RJ, Hammacher A, Smith DK, Matthews JM, Ward LD. Interleukin-6: structure-function relationships. Protein Sci. 1997 May;6(5):929-55. doi: 10.1002/pro.5560060501. PMID: 9144766; PMCID: PMC2143693.

Vaughan VC, Martin P, Lewandowski PA. Cancer cachexia: impact, mechanisms and emerging treatments. J Cachexia Sarcopenia Muscle. 2013 Jun;4(2):95-109. doi: 10.1007/s13539-012-0087-1. Epub 2012 Oct 25. PMID: 23097000; PMCID: PMC3684701.

Webster JM, Kempen LJAP, Hardy RS, Langen RCJ. Inflammation and Skeletal Muscle Wasting During Cachexia. Front Physiol. 2020 Nov 19;11:597675. doi: 10.3389/fphys.2020.597675. PMID: 33329046; PMCID: PMC7710765.

Weledji EP, Enoworock G, Mokake M, Sinju M. How Grim is Pancreatic Cancer? Oncol Rev. 2016 Jul 6;10(1):294. doi: 10.4081/oncol.2016.294. PMID: 27471581; PMCID: PMC4943093.